Postprint of: Trawiński B., Bochentyn B., Kusz B.: A study of a reduction of a micro- and nanometric bismuth oxide in hydrogen atmosphere. THERMOCHIMICA ACTA. Vol. 669, (2018), pp. 99-108. DOI: 10.1016/j.tca.2018.09.010

A study of a reduction of a micro- and nanometric bismuth oxide in hydrogen atmosphere

Bartosz Trawiński*[1], Beata Bochentyn[1], Bogusław Kusz[1]

1. Gdańsk University of Technology, Faculty of Applied Physics and Mathematics, Department of Solis State Physics, ul. G. Narutowicza 11/12 80-233 Gdańsk, Poland

*Corresponding author. E-mail: bartosz.trawinski@pg.edu.pl

ABSTRACT

A reduction of bismuth oxide in hydrogen atmosphere was investigated. The reaction was performed with a material in various structural forms: powder: with micrometric grains, powder with nanometric grains and powder pressed into pellets. The process was performed in both isothermal and non-isothermal conditions. An activation energy of the reaction calculated with Friedman method was found to be about 85 kJ/mol for the reduction of both micrometric powder and pellets. A model fitting analysis based on Coats-Redfern method suggests, that the reaction is limited by a diffusion of gaseous reactants, what is consistent with a structural analysis. An effect of liquid bismuth evaporation was noticed at the beginning of the process. This phenomenon was much stronger in the case of reduction of nanometric powder. The activation energy was estimated to be about 30 – 50 kJ/mol. The reaction could have been performed at lower temperature.

Keywords: bismuth oxide, reduction, hydrogen, kinetics

1. INTRODUCTION

A reduction of metal and metalloid oxides in reducing atmospheres is a way of producing metals and intermetallic alloys and compounds, especially advantageous when elements have different melting points [1]. Reduction with hydrogen is also a method to regenerate metallic catalysts, *e.g.* in carbon nanotubes synthesis [2].

Most of the investigations concerning reduction with hydrogen have been done on transition metal oxides, like *e.g.* iron [3, 4, 5], nickel [6-9], silver [10] cooper [11] or molybdenum [12, 13]. Typically, thermogravimetric analysis is performed in order to determine an extent of the reaction. Using small amount (10-30 mg) of powder forming a thin layer on a microbalance helps to exclude the influence of diffusion outside grains [4, 6, 12]. Experiments can be performed in isothermal or non-isothermal (usually with constant heating rate, up to 30K/min [11]) conditions. For measurements in isothermal conditions, instantaneous gas change in apparatus is required at particular temperature [12]. For this reason, non-isothermal experiments are easier to conduct and more popular.

Methods of kinetic data analysis are well explained by S. Vyazovkin's *et al.* [14, 15]. Additionally, a list of functions describing different reaction mechanism gathered in [6] is helpful. Using different methods of kinetic calculations for the same experimental data can lead to different results [10, 11]. Moreover, in non-isothermal experiments, many different functions can be fit to the experimental data, provided that other kinetic parameters can be freely adjusted during fitting [14]. For isothermal measurements a fitting procedure is more simple and can be performed more accurately. Also differences in structure of the oxide – grains' size, crystal structure defects [3], as well as form of the sample (*e.g.* powder, pellet)

can significantly change a mechanism of the reaction [7]. This induces many difficulties in comparing different studies. In case of the oxide reduction analysis, a Friedman method is applied for the activation energy calculation [4-6, 10]. For the evaluation of the reaction model function, a Coats-Redfern method can be used [3, 6, 10, 13].

An influence of grains aggregation on the reduction process has been investigated for nickel oxide pellets [7] and wires [8]. Data obtained for reduction of pellets was successfully fitted to a "structural model" based on grain sizes as well as on a size and distribution of pores. Additionally, photographs of pellets after partial reaction confirmed a prediction based on the proposed model and a key role of mass transfer. This can be compared to a study of NiO powder reduction [6], which revealed nucleation and growth of Ni particles as a rate-determining step. Investigation of reduction of NiO wires [8] also has shown a significant role of diffusion, however, authors pointed, that at low temperatures (up to 800 K) the rate of grains nucleation and growth is also significant. Kinetic data analysis was supported by SEM imaging with chemical composition analysis. A porous structure was found in partially reduced areas of samples. Ni phase was identified around pores and NiO and bulk areas, again confirming an influence of a mass transport in the reaction kinetics.

A reduction of bismuth oxide was investigated by F. Korkmaz *et al.* [16]. The reaction was conducted with ethanol, decomposing into hydrogen and carbon oxide. That study revealed, that in a low temperature range the reaction rate is limited by kinetics of the reaction itself (nucleation and growth of liquid bismuth particles), while at high temperatures (above 700 K) by a transport of gaseous reactants through the powder bed. It was found, that Bi forms a layer on the surface of Bi_2O_3 particles, which transforms into micrometric Bi droplets growing to milimeters while reaction proceeds. Other study [17] shown that at temperatures lower than 500 K the reaction rate is limited by a transport in a gaseous phase. The reduction of Bi_2O_3 is a single step reaction (no other Bi oxides were found to be stable), however calculations show a possibility of gaseous bismuth hydrides formation. The reduction of bismuth ions by hydrogen in bismuth silicate and germanate glasses has also been previously investigated [18, 19]. It was found, that Bi clusters, with diameters up to 10 nm, are formed in a glass matrix in a layer under the glass surface. Thickness of this layer was found to be 40-50 μm. A migration of Bi atoms to the surface and formation of spherical particles was also noticed. In our previous research a method of oxides reduction with hydrogen has been applied for a synthesis of thermoelectric materials, see [20, 21] and references therein. Similar method was applied by Lee *et al.* for bismuth telluride based materials [22-24]. These studies focused on parameters of the synthesis procedure and properties of materials rather than on the reaction itself. Only "external" factors, like time and temperature have been investigated, without an insight into "internal" reactions mechanisms. In order to investigate the reduction process we decided to firstly investigate an influence of a structure of substrates on the reaction course.

In this study, a reduction of bismuth oxide with hydrogen $Bi_2O_3+3H_2 \rightarrow 2Bi+3H_2O$ is investigated in isothermal and non-isothermal conditions. The reaction is conducted for different forms of the bismuth oxide – micrometric sized powder, the same powder pressed into pellets as well as a ball-milled nanopowder. The results will provide an information about how the form of the oxide influences reaction processes. It is expected, that the higher surface area will enhance kinetics of the reaction. This knowledge will be helpful in designing procedures of materials synthesis with an oxide reduction method. Reaction extent is

measured by a thermogravimetry method. Results of the data analysis are compared with SEM images of reaction's products at different stages of the reaction.

2. EXPERIMENTAL

In order to investigate mechanisms of the reduction of bismuth oxide, thermal gravimetric measurements have been conducted in non-isothermal and isothermal conditions. A custom made experimental setup is presented in Fig. 1. A reduced material was put into stainless steel crucible lined with an aluminium foil. The crucible was placed on the top of a stainless steel rod, transferring load onto a balance (AXIS ALZ120), measuring with a 0.0001 g accuracy. Thermocouple placed inside of the rod measured temperature on its top with a maximum uncertainty equal to 1.6%. A whole apparatus was hermetically closed for the experiments. Tube furnace was used to increase the temperature of the reaction chamber. A lower part of the column was cooled with water. Additionally, silica gel was put in the cooled area of the chamber for capturing of water vapour.

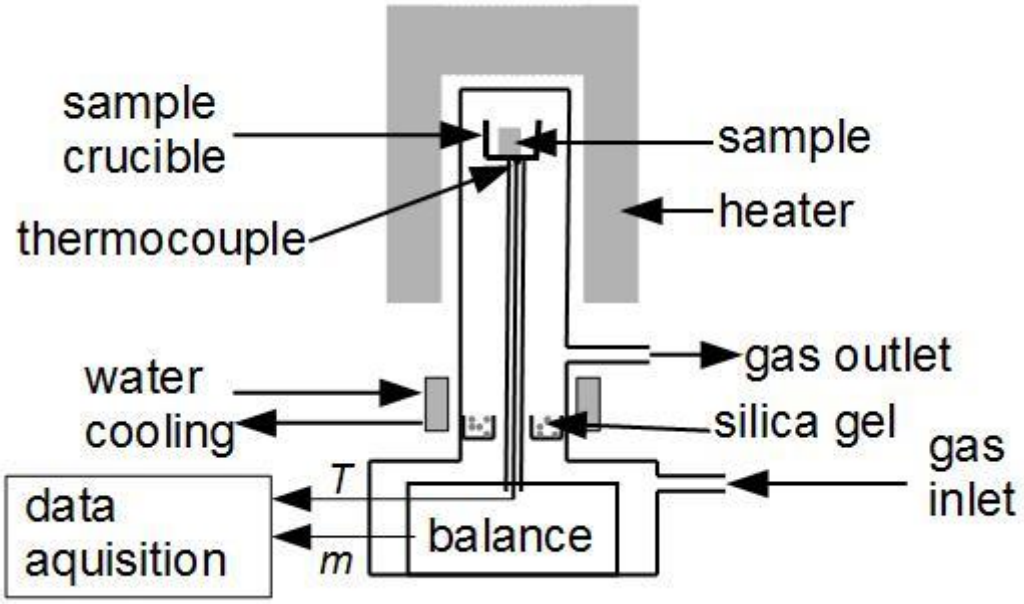

Fig. 1. Scheme of experimental apparatus

Investigation was performed with a bismuth oxide powder from Alfa Aesar (99~~,~~.975%). For experiments with material further called a "powder" it was used without an additional processing. For measurements of a reduction of pellets, the powder was pressed under 520 MPa uniaxial pressure in cylindrical matrix with a diameter of 6 mm. A mass of a reduced material was about 0.85 g in each measurement. Additional experiment was performed with a powder milled in a planetary mill (further called "nanometric powder" or "nanopowder"). SEM images of both powders are provided in Supplementary Information, Figure S1. After closing the apparatus, it was rinsed with nitrogen in order to remove air. After that, the reaction chamber was rinsed with a rapid stream of hydrogen. After rinsing the experiment was started with turning the heater on and a constant 160 ml/min flow of hydrogen was kept. Mass and temperature measurements were performed every 10 seconds until the mass changes stopped. In order to fabricate the partially reduced samples, the reaction was

interrupted when a mass change reached an appropriate value – heater was removed, chamber was rapidly rinsed with nitrogen (hydrogen flow was stopped) and cooled down with a fan. In order to verify results of calculations and to perform low temperature experiments, isothermal reactions were also performed. In these processes the apparatus with sample was heated to the experimental temperature in nitrogen atmosphere. Then, the reaction chamber was rapidly rinsed with hydrogen for about 5 minutes. After that, the gas flow was decreased to the constant value of 160 ml/min and the measurement was started.

Structural investigations of the materials were performed. X-Ray diffraction patterns were obtained with a Philips X'Pert Pro MPD diffractometer. Electron microscopy was done with a FEI Quanta FEG 250 microscope with a secondary electron detector. Elemental analysis was performed with Energy Dispersive X-ray Spectroscopy with an ApolloX SDD detector. Accelerating voltage was 10 kV for imaging and 30 kV for EDS. Surface area of the milled powder was measured with BET analysis using Quantachrome NOVAtouch 1LX instrument at 77 K. Surface area of the other materials was too low to be measured.

3. METHODS OF DATA ANALYSIS

Experimental data was limited to a region of actual reaction (changing mass). Reaction extent α was calculated according to eq.1, where m_0 is initial mass of sample, $m(t)$ – measured mass, m_{ox} – mass of oxygen in initial Bi_2O_3 sample.

$$\alpha = \frac{m_0 - m(t)}{m_{ox}} \tag{1}$$

Reaction rate is described by equation 2, where A is pre-exponential constant, E – activation energy, R – universal gas constant and f – function describing reaction model [11]:

$$\frac{\mathrm{d}\alpha}{\mathrm{d}t} = A\exp\left(\frac{-E}{\mathrm{R}T}\right) f(\alpha) \tag{2}$$

Dependence of α on time (t) was approximated by the 7th order polynomial denoted as α_c. Correlation coefficient R^2 values were at least 0.9995, lower values were obtained for micrometric powder (at least 0.999). Reaction rate ($d\alpha_c/dt$) values were simply obtained from $\alpha_c(t)$.

Supposing that function f is independent from T and α is constant, a linear relation of $\ln(d\alpha/dt)$ on 1/T can be derived from eq. 2:

$$\ln\frac{\mathrm{d}\alpha_c}{\mathrm{d}t} = \ln[Af(\alpha)] - \frac{E}{\mathrm{R}T} \tag{3}$$

Friedman method to calculate activation energy involves a linear regression of a reaction rate and temperature data according to eq. 3. This method was used to calculate E for the reduction of different forms of bismuth oxide. For each α, pairs of corresponding α_c and T (one pair from one measurement) were found and used for calculation of the activation energy. Uncertainty of E was found on the basis of std. deviation of the slope parameter of the regression.

Model fitting of non-isothermal data was performed with a Coats-Redfern method [25]. It was used to fit the obtained data to different functions f for every set of experimental values. This method involves linear regression of measured values (α, T) according to equation 4:

$$\ln\frac{g(\alpha)}{T^2} = \ln[\frac{AR}{\beta E}(1-\frac{2RT_m}{E})] - \frac{E}{RT} \quad (4)$$

T_m is a mean reaction temperature, factor β is a rate of constant temperature change and function g is described by equation 5.

$$g(\alpha) = \int \frac{d\alpha}{f(\alpha)} \quad (5)$$

A set of 20 model functions, presented in Supplementary information, Table S1, was taken from [6]. Function f is well describing the reaction if the experimental data can be fitted to eq. 4 with a high correlation and the calculated activation energy is similar to values estimated by the Friedman method.

4. RESULTS AND DISCUSSION

The reduction of bismuth oxide in different forms has been investigated. Basic information about the used materials is provided in Table 1. The BET results for micropowder and pellets have high uncertainty, due to low surface area.

Table 1. Properties of the reduced materials.

	grain size (with std. deviation)	BET surface area	porosity
micropowder	1.34±0.85 μm	0.3 m^2/g	n.a.
pellet		0.7 m^2/g	(15±2)%
nanopowder	85±45 nm	6.7 m^2/g	n.a.

In order to investigate the process of reduction of Bi_2O_3 powder and pellets in hydrogen, five non-isothermal thermogravimetric experiments have been performed for an each form of oxide. Actual values of heating rates for a powder were equal to 2.0, 3.1, 4.2, 5.3, 7.2 K/min and for pellets were equal to 2.0, 3.2, 4.2, 5.3, 6.8 K/min. Measurement of the reduction of a ball-milled powder has been done with a 2.0 K/min heating rate.

Additional experiments were performed with increased (up to 200 ml/min) hydrogen flow with 5 K/min heating rate for powder and at 292 K (isothermally) for milled powder. The results revealed no influence of the flow rate on the reaction kinetics. Therefore, the 160 ml/min hydrogen flow is not limiting the reduction process.

Comparison of $\alpha(T)$ dependencies measured at 2.0 K/min heating rate for all three forms of bismuth oxide is presented in Fig. 2. While curves for a powder and a pellet are quite similar, the one for a milled powder starts at lower temperature and reaction is faster. This indicates, that nanostructurization and/or introducing defects enhances the reaction, like it has been observed for an iron oxide [3]. Moreover, it can be seen that the mass changes do not finish at 100% of reaction extent. This effect can be explained by a high surface area, promoting an evaporation of bismuth and resulting in the additional mass loss. Further analysis of this effect is provided in sections 4.2 and 4.3. Expecting a lower influence of evaporation at low temperatures, isothermal reactions were performed with a milled powder. Results obtained for a milled powder investigation are discussed separately.

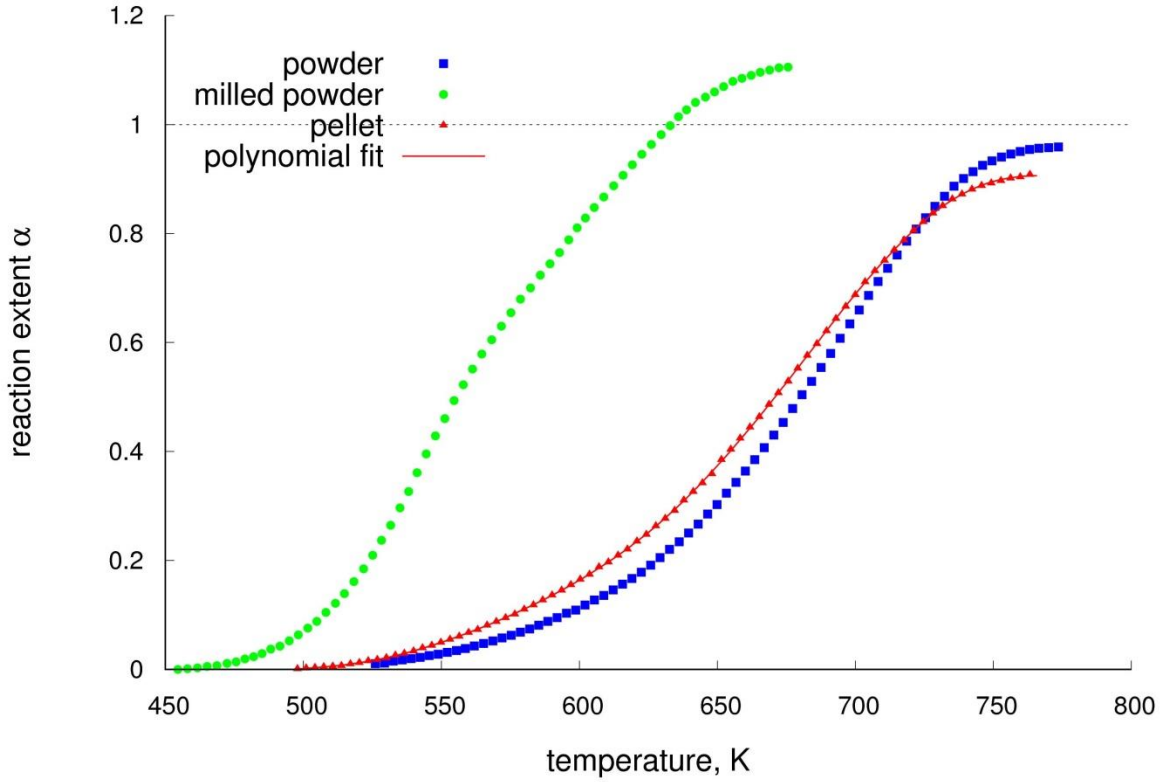

Fig. 2. Dependence of the reaction extent on temperature measured for a powder, a milled powder and a pellet (with calculated polynomial fit) at 2 K/min heating rate; every 10th point is marked

4.1. Structural changes during reaction

In order to perform visual inspection of partially reacted samples, reactions were conducted with 4.2 K/min heating rate and interrupted after observable mass changes started, and after reaching 10, 20, 50 and 75% reaction extent, at temperatures respectively 553, 614, 677, 736, 758 K for a powder and 527, 607, 647, 707, 770 K for pellets.

In the beginning of the powder reduction a sample became grey, but yellow (colour of Bi_2O_3) areas were visible. For 10 and 20% reaction extent the powder was grey and a little darker on the top of the powder bed, indicating some influence of the powder bed depth. At 50% of reaction extent a material was sintered and metallic particles were visible on the top; at 75% they occurred in a whole volume of the powder. Finally, at the end of the reaction, a layer of metallic material was formed on the bottom of the reaction pot, and darker spherical particles were visible at this layer. Photographs of powder and pellet after completed reaction are presented in Fig. 3.

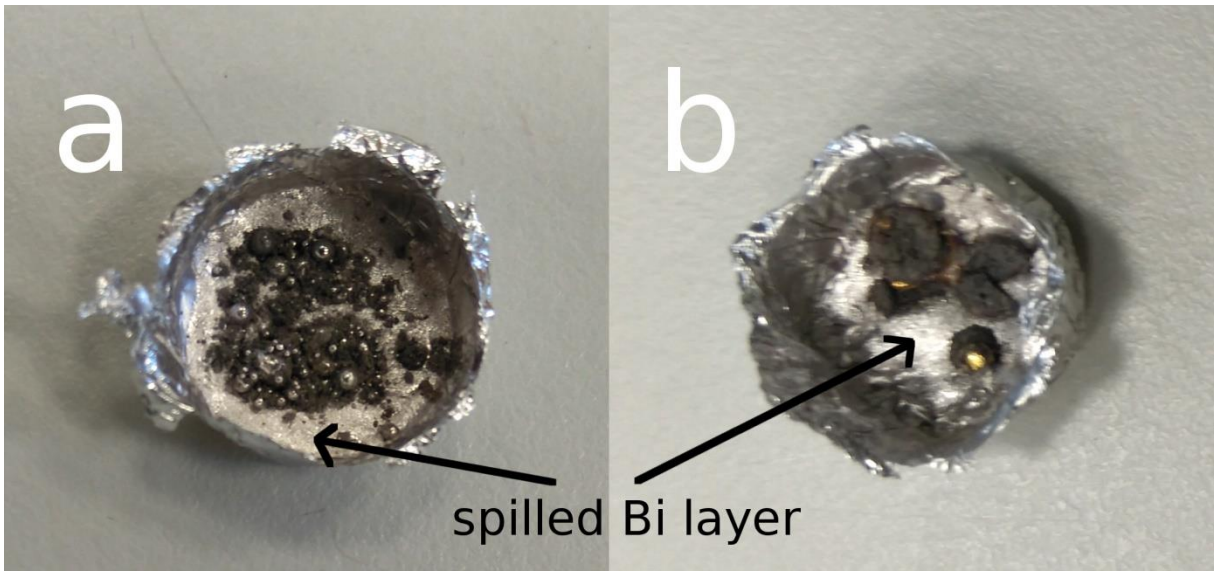

Fig. 3. Photographs of a) powder and b) pellet after completed reduction with 4 K/min heating rate

The SEM images of partially reduced samples and of the one after a completed reaction are presented in Fig. 4. It is visible, that firstly some small particles (with diameter below 100 nm) appear on the surface of oxide grains. During the reaction progress, the particles become larger, covering a whole surface of oxide grains. This process is visible in Fig. 4 a,b,d. The particles were identified as a Bi phase on the basis of Energy Dispersive X-Ray Spectroscopy, results of which indicated an increased concentration of Bi for measurements with an electron beam focused on the particles. Another structure appearing in the material during reduction is visible in Fig. 4c. Small holes are visible at the surface of grains. This indicates, that the mechanism of the reaction may be similar to the one described in [7], where a formation of small pores allowed for transfer of hydrogen and water. Images suggest, that bismuth appears at the surface of oxide grains, due to higher hydrogen availability. In Figures 4e and 4f, presenting the material after over 50% of the reaction, the structure is much less porous, which is consistent with the observed sintering effect. This may be reasoned by a solidification of liquid bismuth during cooling, leading to a formation of a continuous structure, joining oxide grains.

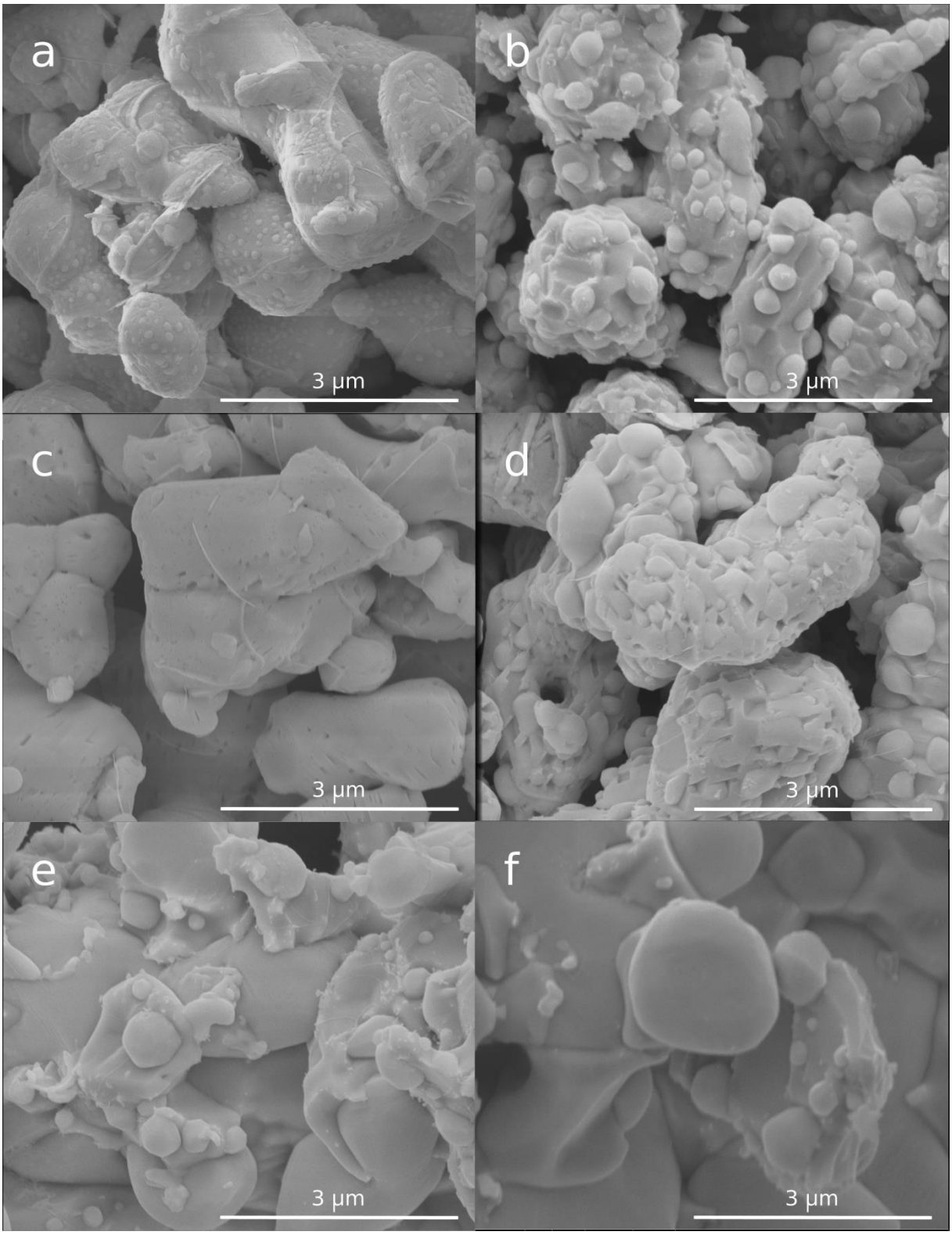

Fig. 4. SEM images of reduced powder after a) reaction initialization – Bi granules visible , b) 10% reaction extent, c) 20%, d) 20% (other area of the sample), e) 50% - continuous Bi structure, f) 75%

Partial reduction experiments have been also performed for bismuth oxide pellets. From the reaction initialization up to 50% of the reaction extent, reduced materials maintained a form of pellets an had grey colour, both on the surface and inside porous tablets. Metallic particles were visible with the naked eye in 50% sample, like it was for a powder. After 75% of the

reaction and after its completion, a layer of solidified metal was visible at the bottom of the crucible with a dark grey pellet residue stuck to the bottom metallic layer, see Fig. 3b. Separate metallic particles occurring after 50% of the reaction were not found. SEM images of partially reduced materials are presented in Fig. 5.

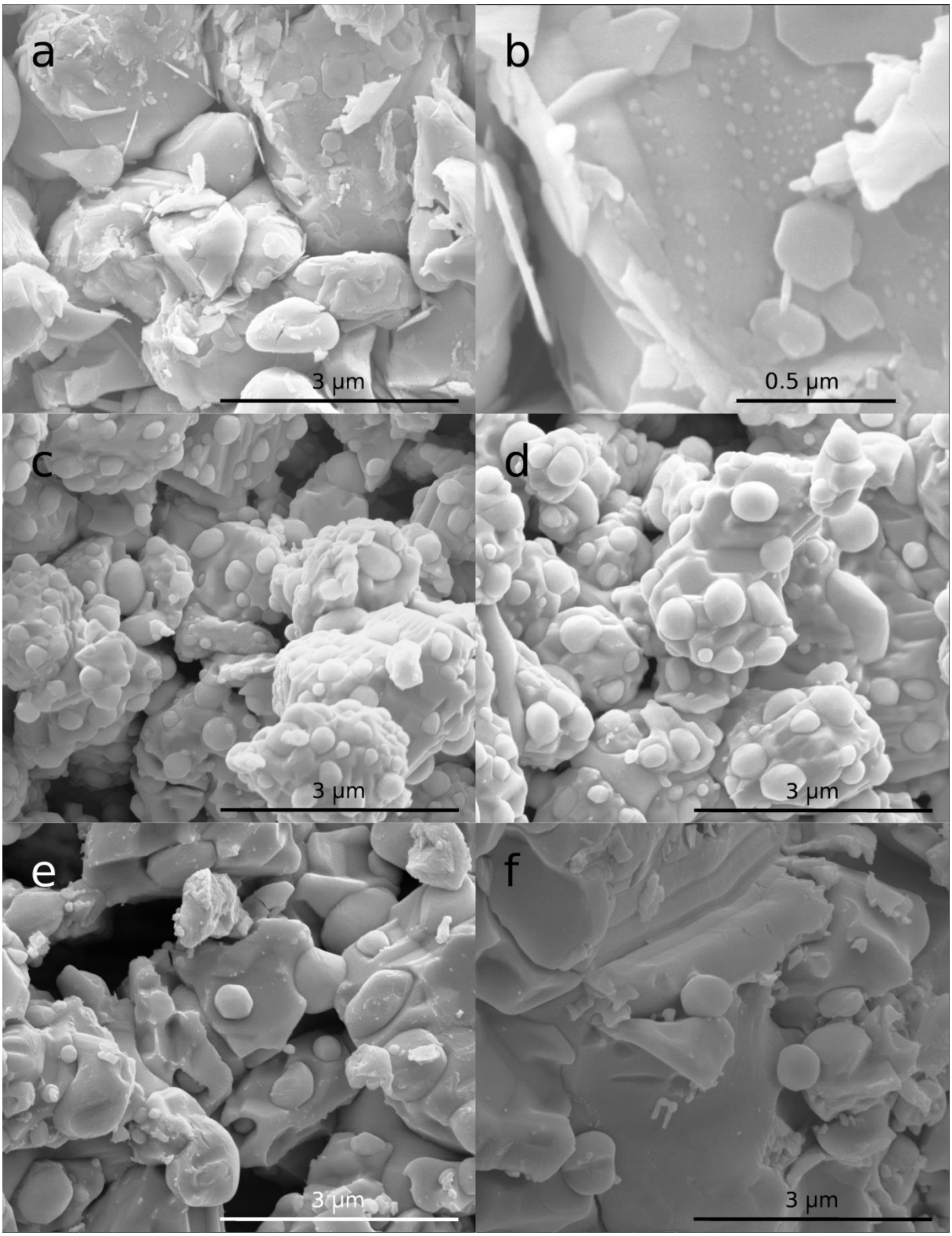

Fig. 5. SEM images of reduced pellets a) and b) after reaction initialization, c) 10%, d) 20%, e) 50%, f) 75%

The structural changes during a reduction process of pellets occur in the same manner as in the powder. Bi nuclei visible in Fig. 5b have diameter below 40 nm. It can be concluded, that the reaction was stopped at the earlier stage than for the powder. Pores between oxide grains are again filled with bismuth phase for the material reduced in 50% reaction extent. Before this happens, pores allow hydrogen to penetrate volume of the sample and process occurs in the same manner in bulk and near the surface.

It can be noticed in Fig. 2, that the reaction extent curve for a powder and a pellet is not reaching 100%. The lowest reached value was 90% for pellets reduced with the heating rate equal to 2 K/min. This sample was divided into two parts – bright metallic spilled at the bottom of the crucible, and dark grey residue (see Fig. 3b). These two parts were milled and examined with a powder X-ray diffraction; results are presented in supplementary information, Fig. S2. Higher concentration of bismuth oxide has been found in the dark pellet residue. This indicates, that the oxide grains prevent liquid bismuth from spilling in the crucible. Instead, bismuth forms a coating on the grains, which probably acts as a diffusion barrier. A similar effect was observed during the reduction of mixed nickel and vanadium oxide [26]. The reduced nickel formed a structure, which blocked transport of hydrogen and consequently prevented the reduction of vanadium oxide.

4.2. Kinetic analysis

Results of measurements of bismuth oxide reduction at different heating rates are presented in Figures 6 and 7, respectively for powder and pellets. Obtained α-T relation show sigmoidal behaviour, typical for non-isothermal reactions [15]. For higher heating rates, the temperature reaches higher values for particular values of the reaction extent. Maximum value of this temperature difference is about 50 K and for this value the assumption of $f(\alpha)$ independence on T should be valid.

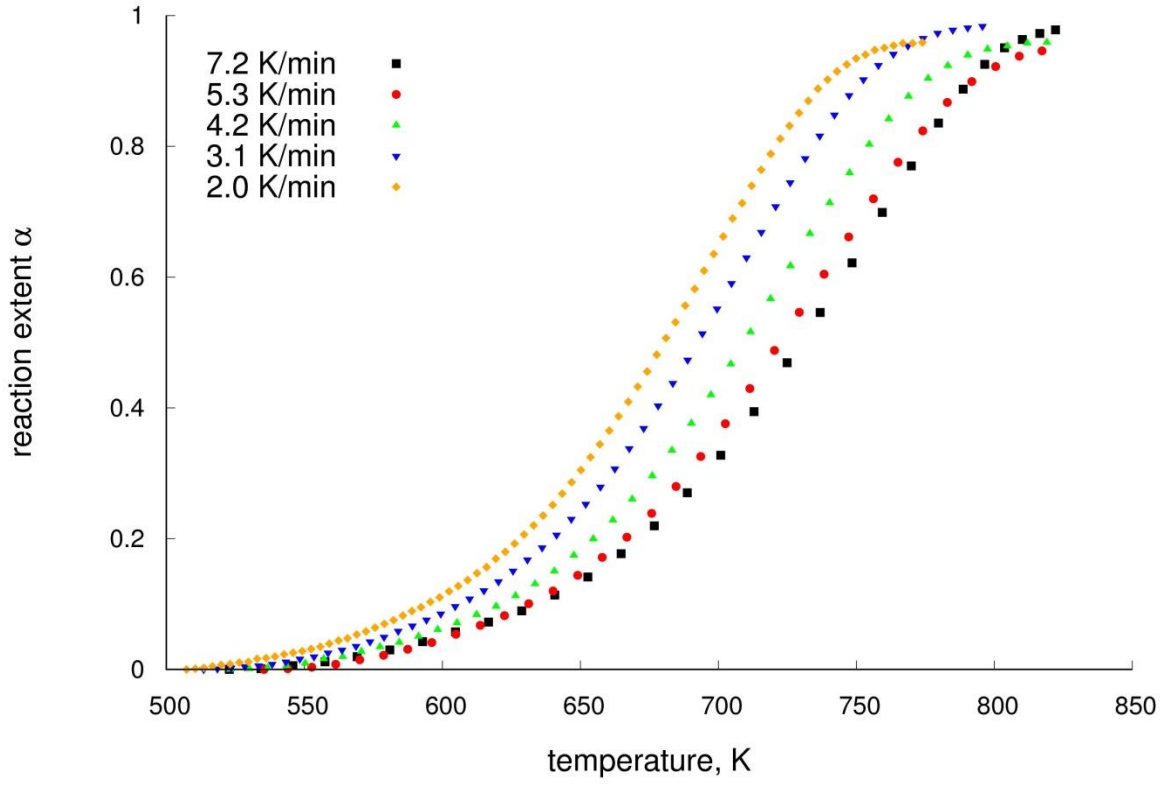

Fig. 6. Dependence of reaction extent on temperature during reduction of powder at different heating rates; every 10th point is marked

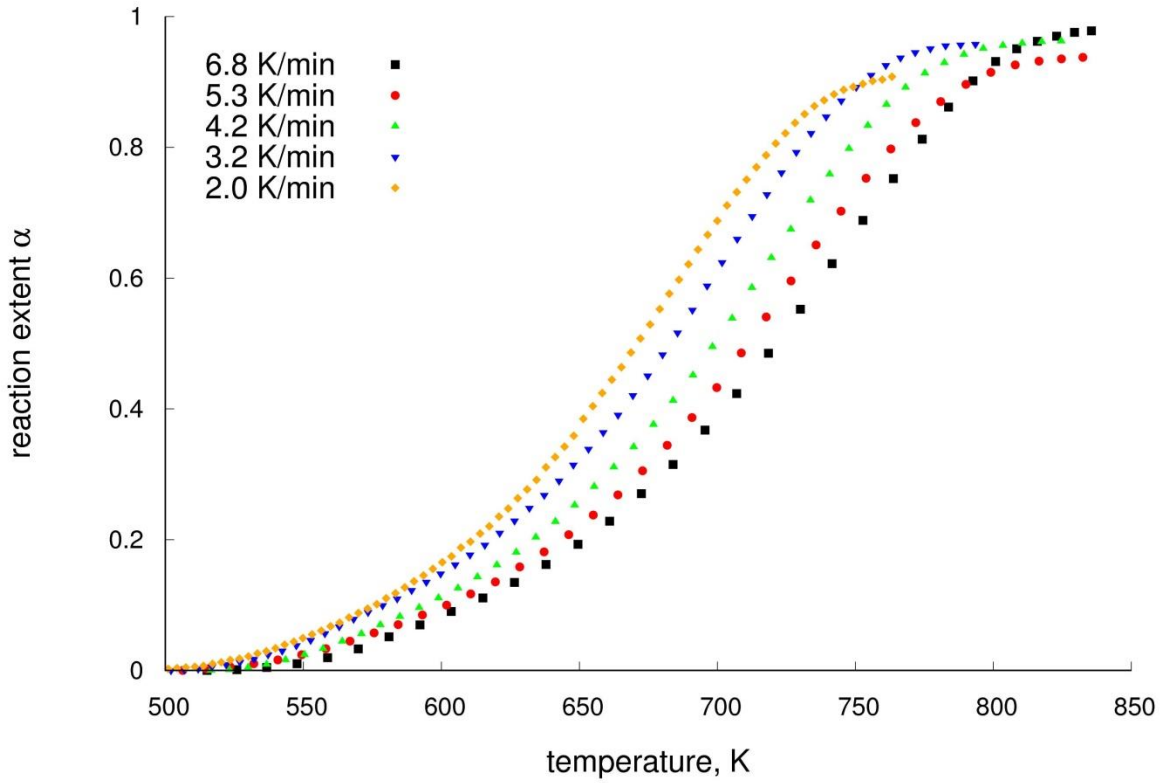

Fig. 7. Dependence of reaction extent on temperature during reduction of pellets with different heating rates; every 10th point is marked

In order to perform kinetic computations, the reaction rate dα/dt has been calculated. This value is plotted against the temperature in Figs. 8 and 9 for a powder and for a pellet reduction respectively. Reactions for both powder and pellet can be separated into two overlapping regions (indicated by overlapping semi circles on the plots), one of which is visible up to about 10% reaction extent, and second above this value. Typically, existence of more than one maximum indicates a multi-step reaction [1, 3]. Here however, the reaction is single-step (no bismuth oxides other than Bi_2O_3 exist). A possible explanation of an increased mass changes at the initial stage is evaporation of Bi nanoparticles occurring on the beginning of the reaction.

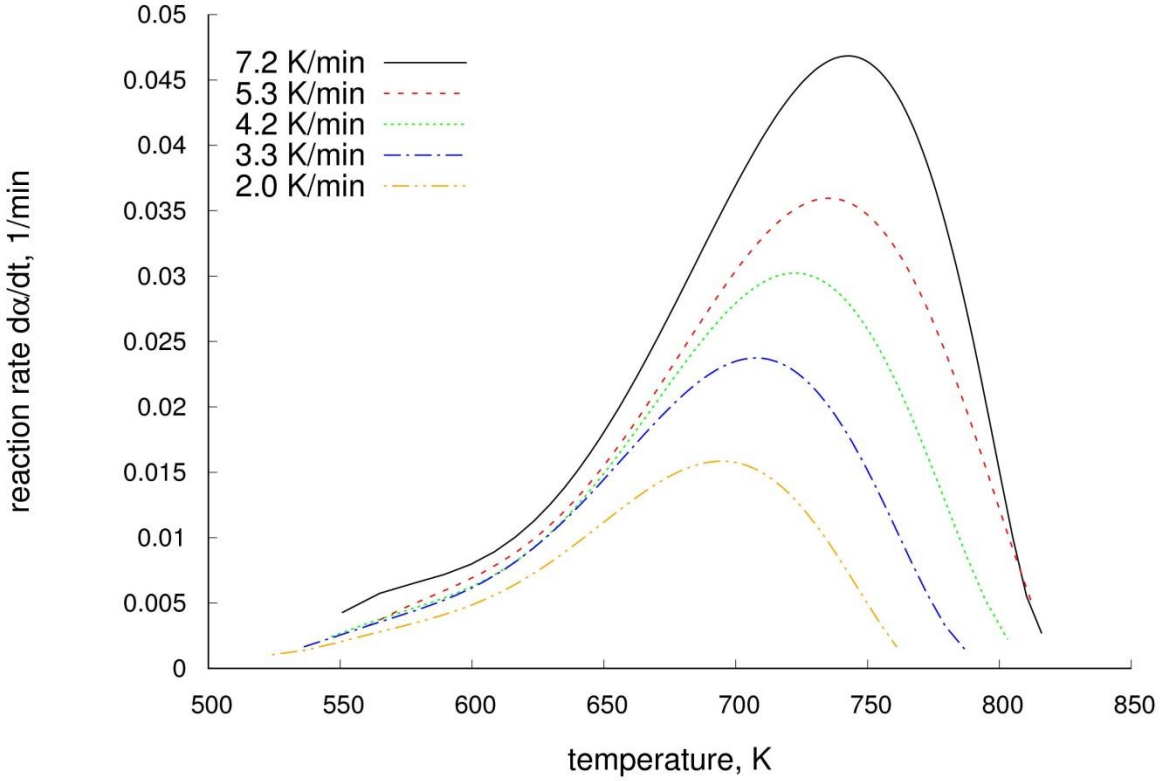

Fig. 8. Dependence of the reaction rate on temperature during reduction of powder with different heating rates

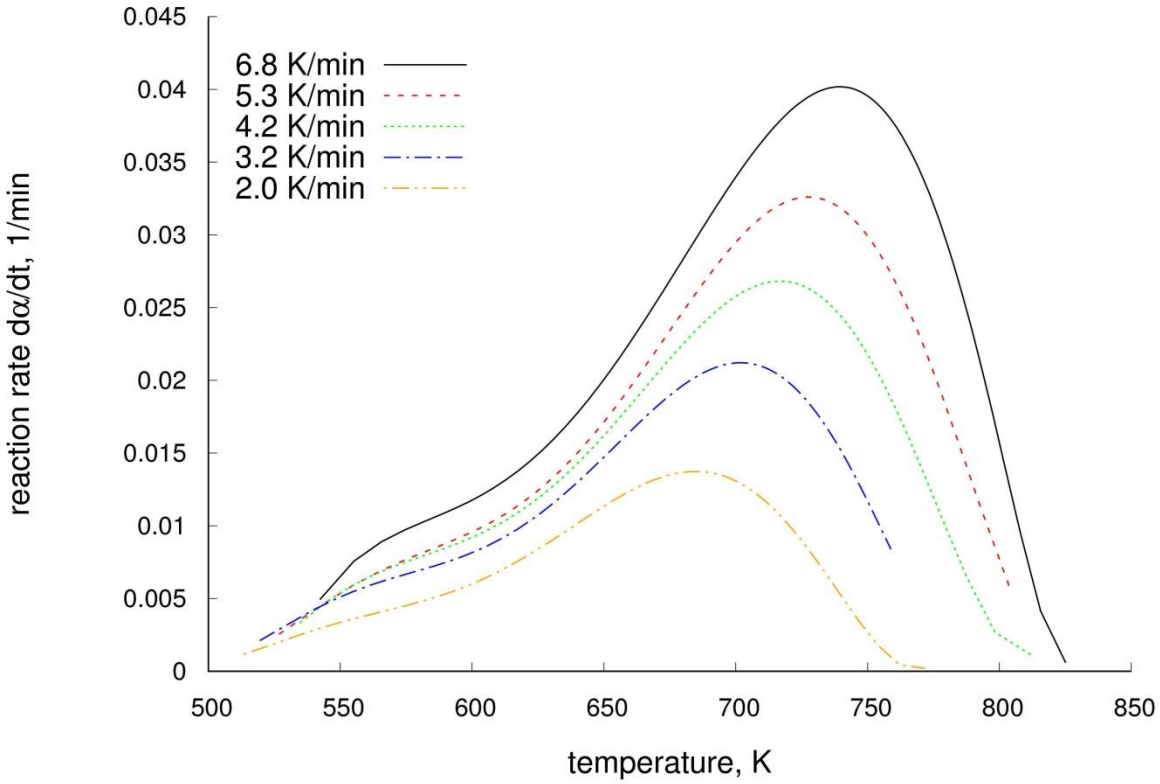

Fig. 9. Dependence of the reaction rate on temperature during reduction of pellets with different heating rates

Maximum values and ends of reactions are shifting to higher temperatures with an increasing heating rate. Also temperatures corresponding to any reaction extent are higher for faster temperature change. Indeed, the reaction rate is dependent on the reaction extent. Plots of this dependence, presented in Figures S3 and S4 in Supplementary information shows that, despite scaling resulting from different temperatures, the reaction rate – reaction extent function is weakly dependent on a heating rate. This supports the assumption that function *f* is, for results discussed in this paper, independent from temperature

The activation energies calculated with the Friedman method as a function of α are presented in Figure 10. Temperature ranges, for which the *E* values are calculated, are also marked. A Durbin-Watson test revealed no evidence for autocorrelation of regression residuals. In a low α range (below 0.15), a calculated effective activation energy for the powder reduction falls from 94 to 76 kJ/mol and increases reaching 87 kJ/mol for α=0.15. For the pellet, in this range of reaction extent, only a decrease from 105 to 80 kJ/mol is observed. This result can be explained by a faster evaporation (resulting in a higher observed reaction rate) of Bi nanostructures at higher temperatures. Therefore, the slope in the Arrhenius plot has a higher value leading to a higher calculated activation energy. For further reaction progress (α=0.15 up to 0.65), the activation energy can be considered constant in terms of uncertainty. Above this range, fluctuations of the calculated activation energy values are observed. However, the uncertainty is also increasing. Activation energies of bismuth oxide reduction, found in earlier research, had values of 41 kJ/mol [17] or 55 kJ/mol [16]. These values were stated to be related with a kinetic of the reduction [16] or with both kinetics and diffusion limiting the reaction rate [17]. The value given by Korkmaz *et al.* [16] was found for a powder with an average grain diameter equal to 190 nm, what has a significant influence on the activation energy. Chernogorenko and Lynchak [17] do not provide characteristic of the raw material and calculation methods.

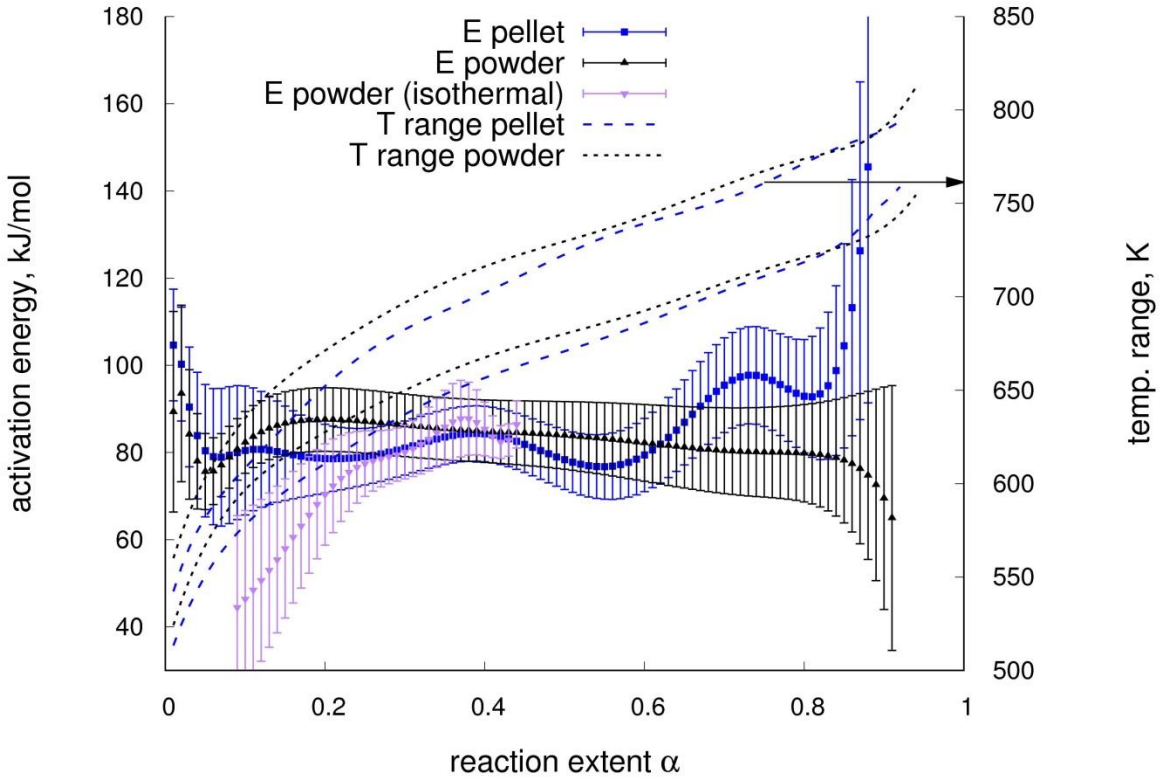

Fig. 10. Dependence of activation energy on reaction extent for powder and pellets; corresponding temperature ranges are marked for non-isothermal conditions

The measured reaction rate dependence on temperature and calculated activation energy show no significant difference between samples in the form of micropowder or pellets. This suggests, that pores in the pellets provide access of hydrogen similarly to the free space in powder.

For a model fitting analysis, the Coats-Redfern method was used to fit the experimental data to 20 different model functions. An initial step with a significant evaporation was deleted from the fitted data. A model selection procedure was performed as follows: for each of 5 runs, the data was fit to 20 models, an average activation energy and an average correlation coefficient for every model were calculated.

In the case of a powder reduction the applied model selection method leads to a conclusion, that models describing 1st and 3/2 order reaction, best fit to the experimental data. In case of the reduction of pellets, 3/2 order reaction and 3D diffusion functions best fit to the experimental data. Models describing 3D diffusion are consistent with SEM and XRD analysis, which have shown significance of a diffusion of hydrogen and water vapour through Bi phase, especially for a reaction extent above 50%. Result of the model fitting procedures are pesented in the Supplementary information, Figures S5 and S6.

For additional validation of model fitting results, the isothermal experiments were performed on the reduction of Bi_2O_3 powder. One measurement was performed at 562 K temperature, about 50 K higher than the reaction initiates. The reaction was interrupted after 5 hours, reaching 44% of conversion. The second experiment was performed at 641 K. At this temperature 11-26% of the reaction extent was reached in non-isothermal experiments. The third reaction was performed at 727 K, which is corresponding to 49-84% reaction extent,

depending on the heating rate. Due to a high temperature, the latter reached significant 46% extent during initial rinsing in hydrogen. Reaction rate ($d\alpha_c/dt$) values for isothermal experiments are presented in Fig. 11. The 562 K plot has two linear fragments, separated for α=0.2. For the reaction extent of 0.4 another change in the character of the function appears. Similar dependence can be observed for the results obtained at 602 K. The characteristic for high temperature (727 K) experiment is even more complicated. An occurrence of function maximum is typical for Avrami-Erofe'ev models; however there is only one maximum. The 641 K temperature measurement shows that reaction rate dependence on α varies with temperature. Consequently, a function *f* is also dependent on the reaction temperature. Therefore, on the basis of isothermal experiments results it can be stated that the investigated process is complex and cannot be described by a single model. Moreover, it can be noticed, that the higher is the temperature, the higher oxide conversion can be reached until the reaction is quenched by the diffusion barrier.

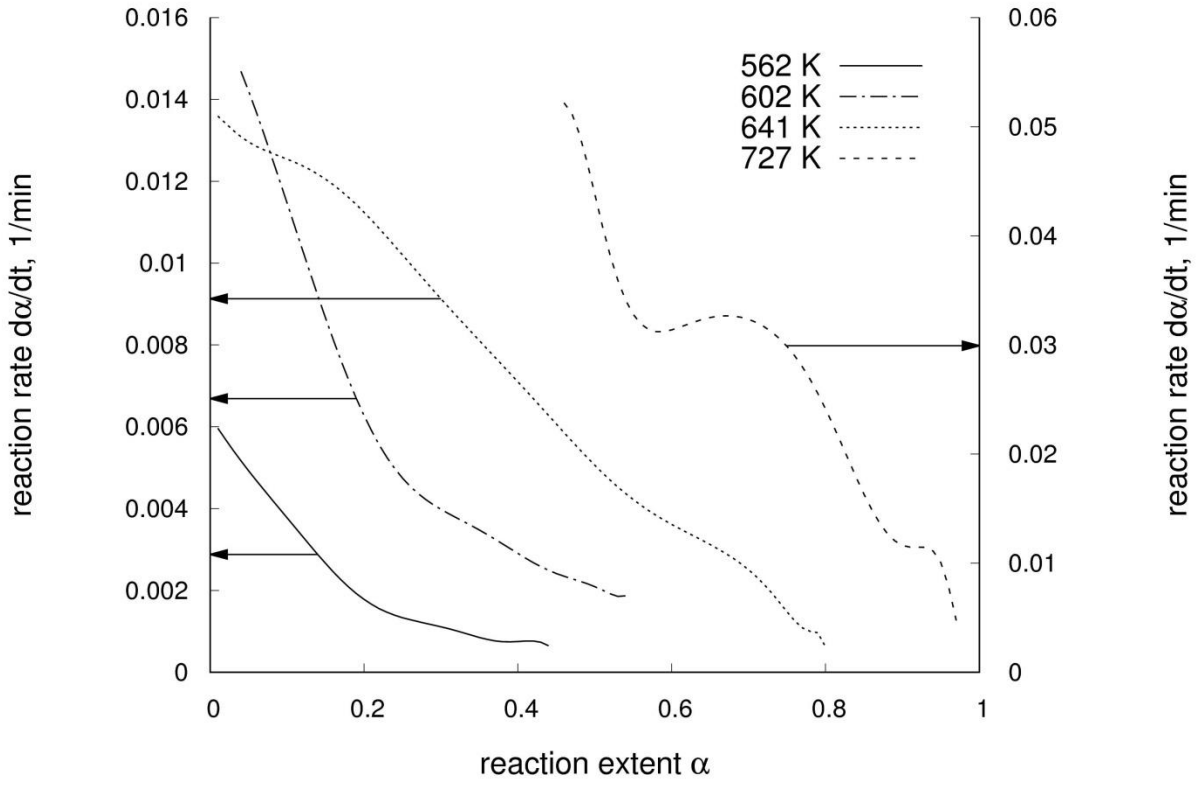

Fig. 11. Dependence of the reaction rate on the reaction extent during reduction of powder in isothermal experiments

At the beginning of the process, faster reaction at 602 K than at 641 K suggests different mechanisms occurring during rinsing, which can be related with local temperature shifts. Therefore, the activation energy values obtained on the basis of isothermal measurements performed at 562 – 641 K (presented in Fig. 10) wasn't calculated for the initial part. In the range of uncertainty, activation energy from isothermal and non-isothermal powder treatment are in agreement. However, initial lower values obtained from isothermal experiments can be explained by a heat treatment in low oxygen partial pressure (nitrogen atmosphere) before the actual reduction. This could change the structure of the surface. This effect was reported in the literature as playing a crucial role in NiO reduction [27].

4.3. Results for a material with nanometric grains

In the case of the nanometric powder, a significant evaporation of bismuth, indicated in Fig. 2 by excessing 100% of the reaction rate (based on a mass measurement), has been observed. The evaporation had to occur from the reduced phase, as bismuth oxide is known to be thermally stable in the investigated temperature range [28]. However, the reaction terminated at 110% of calculated extent and a structure of the reduced material was similar to that of a reduced micrometric powder (Fig. 3a). Therefore it can be concluded, that the evaporation effect takes place at the beginning of the process and is enhanced by a high surface area of the oxide. The reduction process was investigated in isothermal conditions at 506, 535 and 565 K. Reactions were interrupted, when the reaction rate has fallen below 0.005 1/min or lower. A calculated dependence of the reaction rate on the reaction extent is plotted in Fig. 12. For comparison, an isothermal experiment was performed with micrometric powder at 516 K. The result is also plotted in Fig. 12. This figure shows a significant decrease of the temperature necessary for the investigated process as well as enhancement of the reaction rate. Dependence of the reaction rate on α is presented in Supplementary Information, Fig. S7.

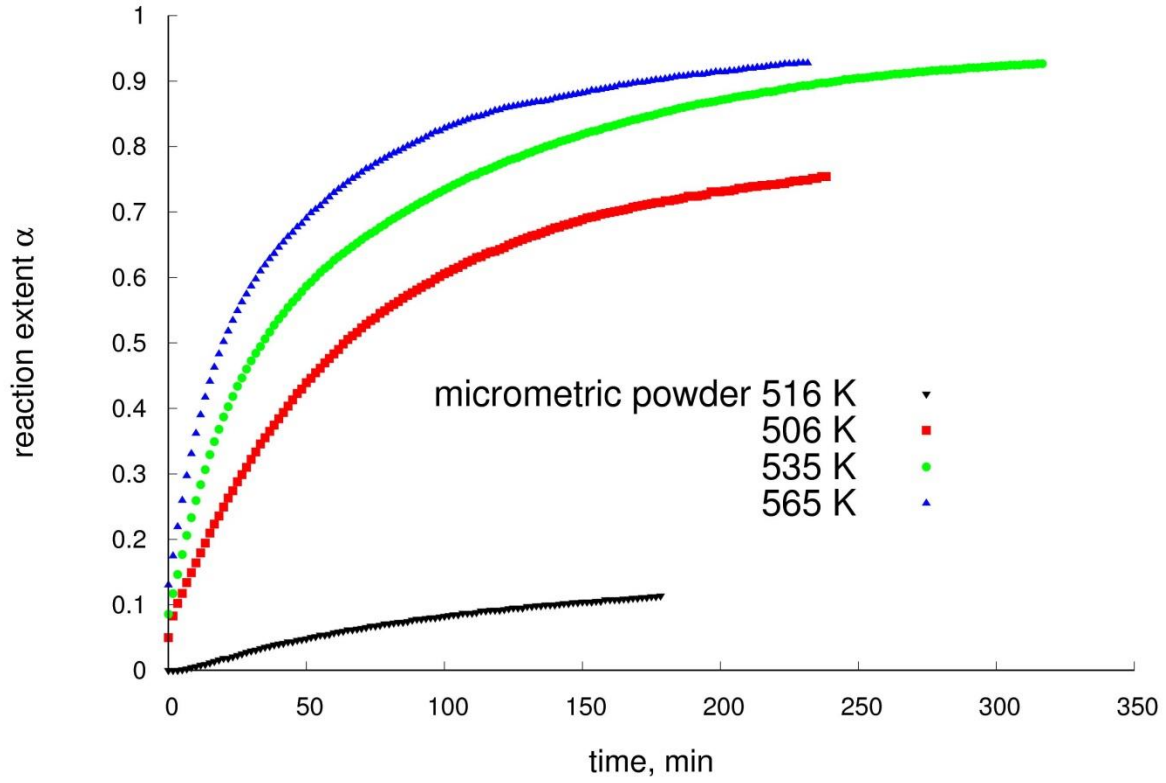

Fig. 12. Dependence of the reaction extent on time during a reduction of a milled nanometric powder in isothermal experiments; result for the initial micrometric powder are added for comparison

In the case of measurements performed at 506 and 535 K, after the reaction was interrupted, materials maintained a bulk structure of the powder. Grains were weakly joined by a metallic bismuth and some sub-milimeter particles with a metallic shine were visible after the reaction at 535 K. The material reduced at 565 K had a structure typical for a powder reduced in non-isothermal conditions. Comparison of these observations with structural changes of micrometric powder leads to a conclusion, that the actual oxide conversion is lower for a

sample reduced at 535 K. Therefore, in the case of this sample, the evaporation effect leads to a higher mass loss, than for a material reduced at 565 K (calculated α values are similar). Consequently, it can be stated, that conducting the reaction at lower temperature promotes a vaporization of bismuth. The evaporation effect is smaller in the case of a micrometric powder because the reaction started at higher temperature and Bi particles joined each other forming grains with a higher surface area.

The SEM analysis was carried out on nanometric powder after reactions at 506 K. The obtained image is presented in Fig. 13. Many small particles are visible. Similarly to the initiation of the reduction of powder or pellets, bismuth is vaporised from these particles. Such small particles are not visible in images in the paper of Korkmaz et al. [16], probably due to higher reaction temperatures (600 – 800 K). Consequently, evaporation didn't occurred in that study.

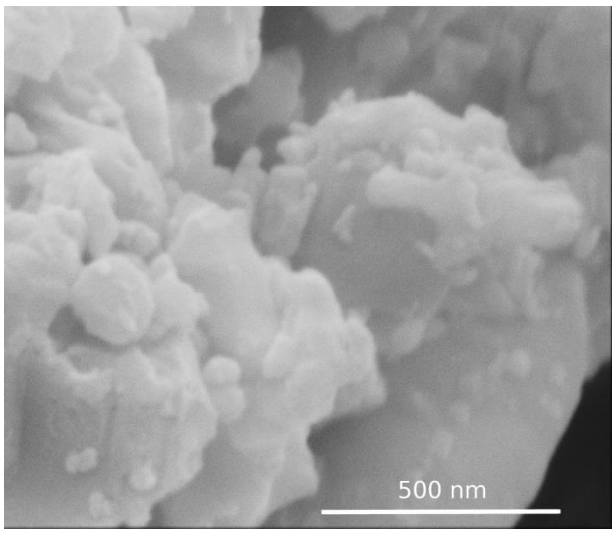

Fig. 13. SEM image of nanopowder reduced at 506 K

Activation energy calculations were performed with the acquired data, similarly to the powder and pellets calculations. The obtained values are presented in Fig. 14. The results are significantly influenced by the evaporation of Bi. This effect shifts the actual reaction extent values, for which E is calculated, as well as increases the reaction rate $d\alpha/dt$ in the equation (3). The calculated values are even lower than these obtained for a powder with 190 nm grains size [17]. For a reaction extent higher than 0.6, the activation energy start to increase. This can be explained by a change of a rate limiting step to the diffusion mechanism, like it was found for the micromeric powder.

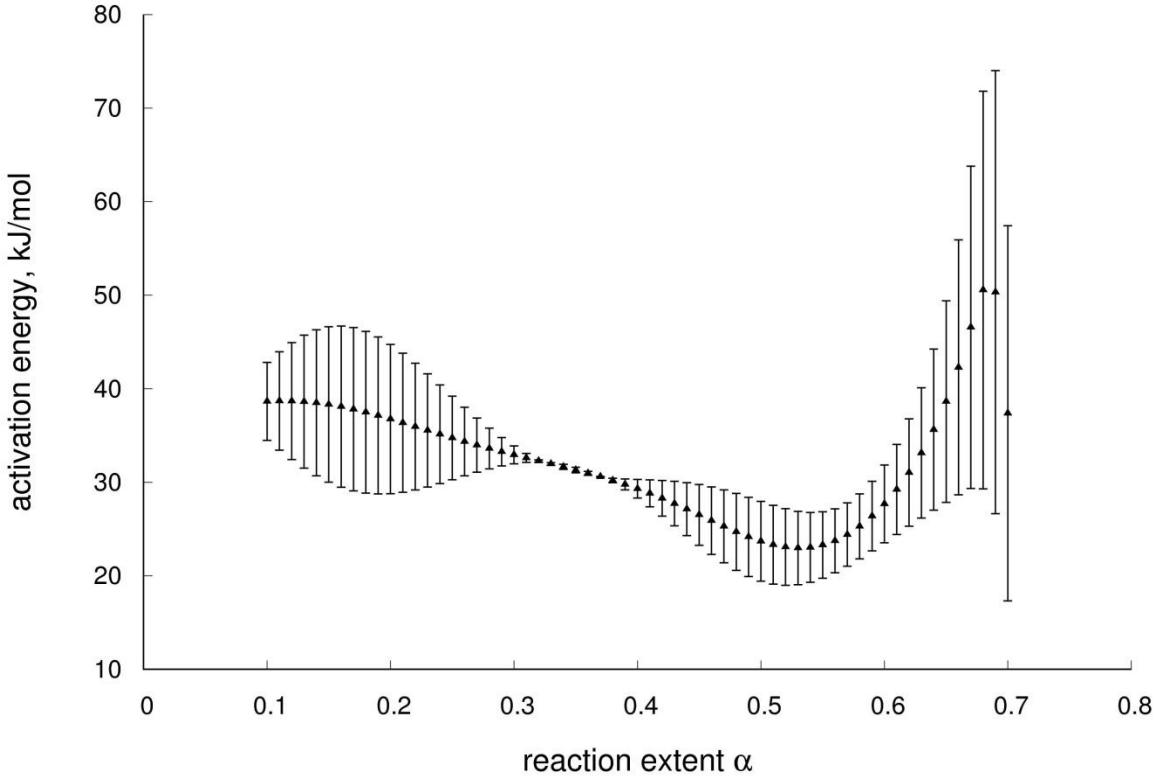

Fig. 14. Dependence of activation energy on a reaction extent obtained for a nanometric powder in isothermal conditions, 506-565 K

5. CONCLUSIONS

The process of bismuth oxide reduction in hydrogen atmosphere has been investigated. The research was performed for the material in forms of micrometric powder, powder pressed into pellets and a ball-milled powder with nanometer sized grains.

For a powder and a pellet the reaction occurred in a similar way. Structural investigations revealed, that Bi phase appears as particles at oxide grains surface. During reaction progress the grains are growing, forming a layer of bismuth, which further transforms into continuous structure with embedded oxide grains. Liquid Bi acts as a diffusion barrier for gaseous reactants, leading to a significant decrease of the reaction rate. A part of the oxide remains unreduced.

Kinetic analysis was performed with the data from non-isothermal experiments. The activation energy was found to be equal to 85±10 kJ/mol. Fitting of different reaction models to the data shown, that in case of powder the 3/2 or 1st order reactions are best describing the investigated process. For reduction of the pellet, 3/2 order reaction as well 3D diffusion models are most accurate.

Results of isothermal experiments shown, that the investigated reactions can't be fully described by a one simple model. Moreover, actual model function is not fully independent from temperature.

Reduction of a ball-milled powder was strongly influenced by the evaporation of bismuth. A reaction extent calculated on the basis of measured mass changes exceeded 100%. The

evaporation effect has been also observed at the initial stage of micrometric powder reduction. Performing the reduction at low temperature promotes the evaporation.

The activation energy calculated from isothermal experiments for the reduction of milled powder is lower than for that with micrometric grains. Reduction of bismuth oxide with small particles can be performed at lower temperature, than in case of micrometre sized grains.

ACKNOWLEDGEMENTS

The authors would like to acknowledge Dr Tadeusz Miruszewski for XRD measurements and Ms Małgorzata Nadolska for BET analysis. This work was supported by the National Science Centre Poland under the grant No. 2016/21/B/ST8/03193.

Declarations of interest: none.

REFERENCES

1. J. C. Juarez, R. Morales, *Reduction Kinetics of Ag_2MoO_4 by Hydrogen*, Metall. Mater. Trans. B 39B (2008) 738-745 doi:10.1007/s11663-008-9173-3

2. M. Kumar, Y. Ando, *Chemical Vapor Deposition of Carbon Nanotubes: A Review on Growth Mechanism and Mass Production*, J. Nanosci. Nanotechnol. 10(6) (2010), 3739–3758 doi:10.1166/jnn.2010.2939

3. P. Pourghahramani, E. Forssberg, *Reduction kinetics of mechanically activated hematite concentrate with hydrogen gas using nonisothermal methods*, Termochim. Acta 454 (2007) 69-77 doi:10.1016/j.tca.2006.12.023

4. K. Piotrowski *et al.*, *Effect of gas composition on the kinetics of iron oxide reduction in a hydrogen production process*, Int. J. Hydrog. Energy 30 (2005) 1543-1554 doi:10.1016/j.ijhydene.2004.10.013

5. H. Chen *et al.*, *Reduction of hematite (Fe_2O_3) to metallic iron (Fe) by CO in a micro fluidized bed reaction analyzer: A multistep kinetics study*, Powder Technol. 316 (2017) 410-420 doi:10.1016/j.powtec.2017.02.067

6. B. Janković *et al.*, *The kinetic analysis of non-isothermal nickel oxide reduction in hydrogen atmosphere using the invariant kinetic parameters method*, Thermochim. Acta 456 (2007) 48–55 doi:10.1016/j.tca.2007.01.033

7. J. Szekely, J. W. Evans, *Studies in gas-solid reactions: Part II. An experimental study of nickel oxide reduction with hydrogen*, Metall. Trans. 2 (1971) 1699-1710 doi:10.1007/BF02913896

8. K. V. Manukyan *et al.*, *Nickel Oxide Reduction by Hydrogen: Kinetics and Structural Transformations*, J. Phys. Chem. C 119 (2015) 16131−16138 doi: 10.1021/acs.jpcc.5b04313

9. P. Erri, A. Varma, *Diffusional Effects in Nickel Oxide Reduction Kinetics*, Ind. Eng. Chem. Res. 48 (2009) 4–6 doi: 10.1021/ie071588m

10. D. Jelić *et al.*, *A thermogravimetric study of reduction of silver oxide under non-isothermal conditions*, Contemp. Mater. I−2 (2010) 144-150 doi:10.5767/anurs.cmat.100102.en.144J

11. D. Jelić *et al.*, *A kinetic study of copper(II) oxide powder reduction with hydrogen, based on thermogravimetry*, Thermochim. Acta 521 (2011) 211-217 doi:10.1016/j.tca.2011.04.026

12. W. V. Schulmeyer, H. M. Ortner, *Mechanisms of the hydrogen reduction of molybdenum oxides*, Int. J. Refract. Metals Hard Mater. 20 (2002) 261–269 doi:10.1016/S0263-4368(02)00029-X

13. B.-S. Kim *et al.*, *Study on the Reduction of Molybdenum Dioxide by Hydrogen*, Mater. Trans. 49(9) (2009) 2147-2152 doi:10.2320/matertrans.MER2008103

14. S. Vyazovkin, C. A. Wight, *Model-free and model-fitting approaches to kinetic analysis of isothermal and nonisothermal data*, Thermochim. Acta 340-341 (1999) 53-68 doi.org/10.1016/S0040-6031(99)00253-1

15. S. Vyazovkin *et al.*, *ICTAC Kinetics Committee recommendations for performing kinetic computations on thermal analysis data*, Thermochim. Acta 520 (2011) 1-19 doi:10.1016/j.tca.2011.03.034

16. F. Korkmaz *et al.*, *Thermodynamic Analysis and Reduction of Bismuth Oxide by Ethanol*, Metall. Mater. Trans. B 47B (2016) 2378-2385 doi:10.1007/s11663-016-0686-x

17. V. B. Chernogorenko, K. A. Lynchak, *Production of bismuth powder by the reduction of bismuth oxide with a mixture of molecular and atomic hydrogen*, Powder Metall. Met. Ceram. 12 (1973) 360-362 doi:10.1007/BF00791258

18. B. Kusz *et al.*, *Structural studies and melting of bismuth nanocrystals in reduced bismuth germanate and bismuth silicate glasses*, J. Non-Cryst. Solids 328 (2003) 137-145 doi:10.1016/S0022-3093(03)00466-6

19. B. Bochentyn *et al.*, *Characterization of structural, thermal and mechanical properties of bismuth silicate glasses*, J. Non-Cryst. Solids 439 (2016) 51-56 doi:10.1016/j.jnoncrysol.2016.02.026

20. B. Trawiński *et al.*, *Structure and thermoelectric properties of bismuth telluride—Carbon composites*, Mater. Res. Bull. 99 (2018) 10-17 doi:10.1016/j.materresbull.2017.10.043

21. B. Bochentyn *et al.*, *Novel method of metal – oxide glass composite fabrication for use in thermoelectric devices*, Mater. Res. Bull. 76 (2016) 195-204 doi:10.1016/ j.materresbull.2015.12.018

22. G.-G. Lee *et al.*, *Synthesis of Bi-Te-Se-based Thermoelectric Powder by an Oxide-Reduction Process*, Electron. Mater. Lett. 6(3) (2010) 123-127 doi:10.3365/eml.2010.09.123

23. G.-G. Lee, G.-H. Ha, *Synthesis of Bi0.5Sb1.5Te3 Thermoelectric Powder Using an Oxide-Reduction Process*, J. Electron. Mater. 43(6) (2014) 1697-1702 doi:10.1007/s11664-013-2846-y

24. Y. S. Lim *et al.*, *Synthesis of n-type $Bi_2Te_{1-x}Se_x$ compounds through oxide reduction process and related thermoelectric properties*, J. Eur. Ceram. Soc. 37 (2017) 3361-3366 doi:10.1016/j.jeurceramsoc.2017.04.020

25. A. W. Coats, J. P. Redfern, *Kinetic Parameters from Thermogravimetric Data*, Nature 201 (1964) 68-69 doi:10.1038/201068a0

26. M. Pospišil, *Study of reduction kinetics of mixed oxides NiO-V2O5 with hydrogen*, J. Thermal Anal. 27(1) (1983) 77-87 doi:10.1007/BF01907323

27. J. A. Rodriguez *et al.*, *Experimental and Theoretical Studies on the Reaction of H2 with NiO: Role of O Vacancies and Mechanism for Oxide Reduction*, J. Am. Chem. Soc. 124(2) (2002) 346-354 doi:10.1021/ja0121080

28. G. Guenther, O. Guilllon, *Solid state transitions of Bi2O3 nanoparticles*, J. Mater. Res. 29(12) (2014) 1383-1392 doi:10.1557/jmr.2014.124

SUPPLEMENTARY INFORMATION

TABLE S1. List of reaction models used for fitting [5]

		model	function *f*
power models	1	power 3/4	$4\alpha^{3/4}$
	2	power 2/3	$3\alpha^{2/3}$
	3	power 1/2	$2\alpha^{1/2}$
	4	power -1/2	$(2/3)\alpha^{-1/2}$
reaction order models	5	0. order	1
	6	1. order	$1-\alpha$
	7	3/2. order	$(1-\alpha)^{3/2}$
	8	2. order	$(1-\alpha)^{2}$
	9	3. order	$(1-\alpha)^{3}$
phase boundary control models	10	2D	$2(1-\alpha)^{1/2}$
	11	3D	$3(1-\alpha)^{2/3}$
Avrami-Erofe'ev nucleation and growth models	12	order 1/2	$(1/2)(1-\alpha)[-\ln(1-\alpha)]^{-1}$
	13	order 3/2	$(3/2)(1-\alpha)[-\ln(1-\alpha)]^{1/3}$
	14	order 2	$2(1-\alpha)[-\ln(1-\alpha)]^{1/2}$
	15	order 3	$3(1-\alpha)[-\ln(1-\alpha)]^{2/3}$
	16	order 4	$4(1-\alpha)[-\ln(1-\alpha)]^{3/4}$
diffusion models	17	1D	$1/(2\,\alpha)$
	18	2D	$1/[-\ln(1-\alpha)]$
	19	3D Jander	$3(1-\alpha)\text{^}(1/3)/\{2[(1-\alpha)\text{^}(-1/3)-1]\}$
	20	3D Ginstling–Brounshtein	$(3/2)[(1-\alpha)\text{^}(-1/3)-1]$

FIGURE S1. SEM images of a) micrometric powder and b) nanometric powder used in the experiments

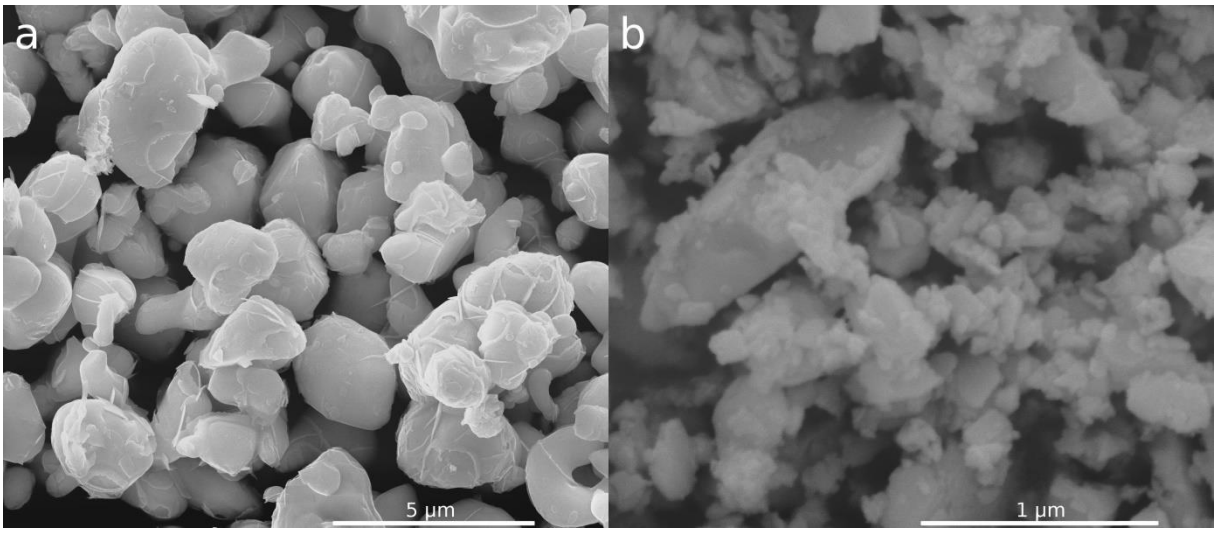

FIGURE S2. XRD patterns of two parts of pellets reduced at 2 K/min heating rate

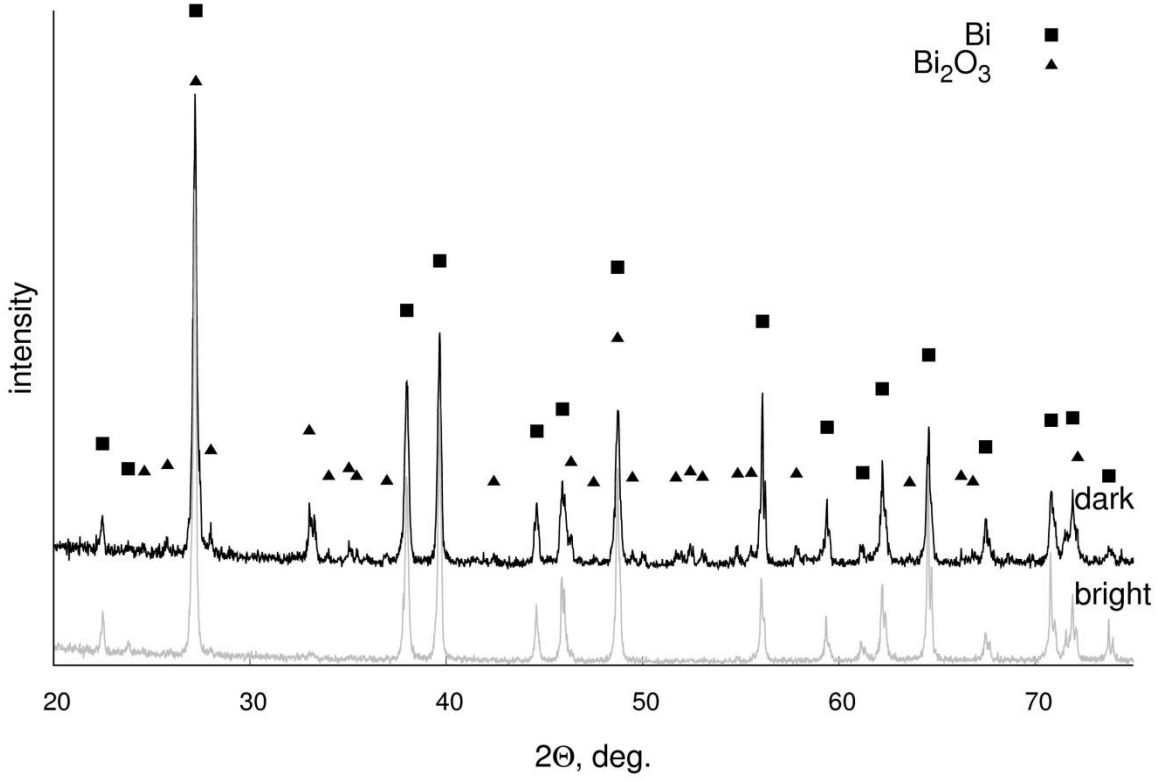

Patterns obtained with CuKα radiation.

FIGURE S3. Dependence of the reaction rate on the reaction extent during reduction of powder with different heating rates

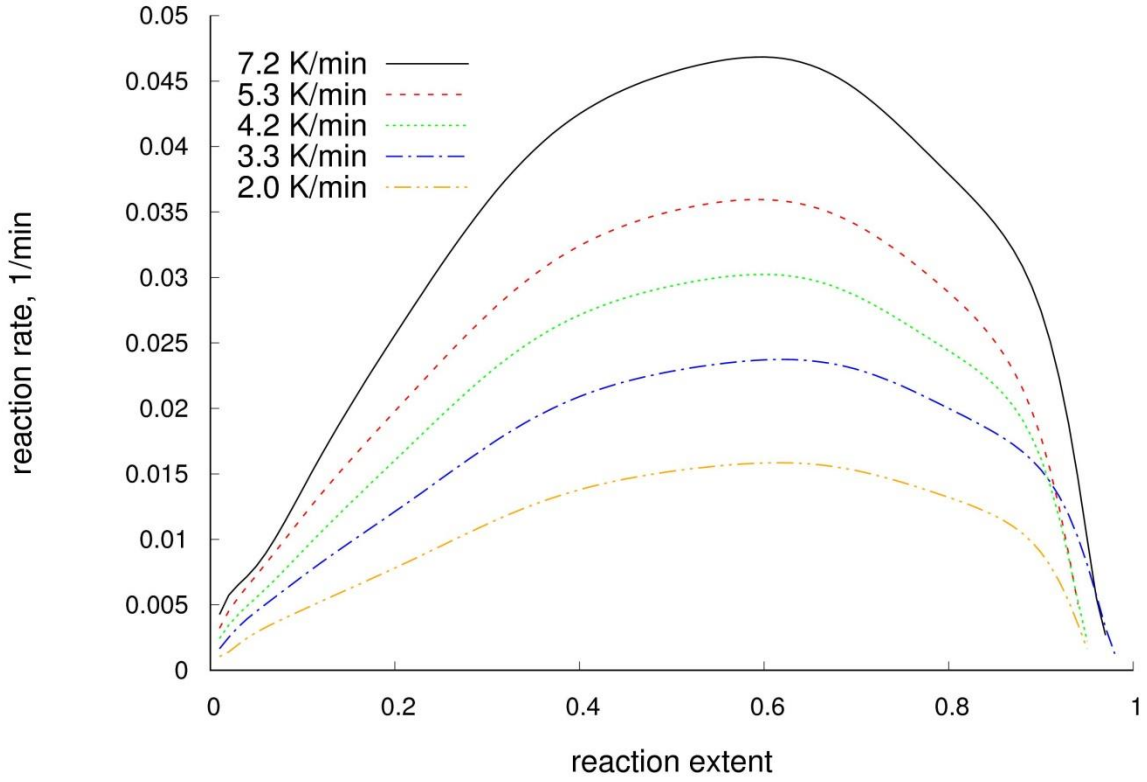

FIGURE S4. Dependence of the reaction rate on the reaction extent during reduction of pellets with different heating rates

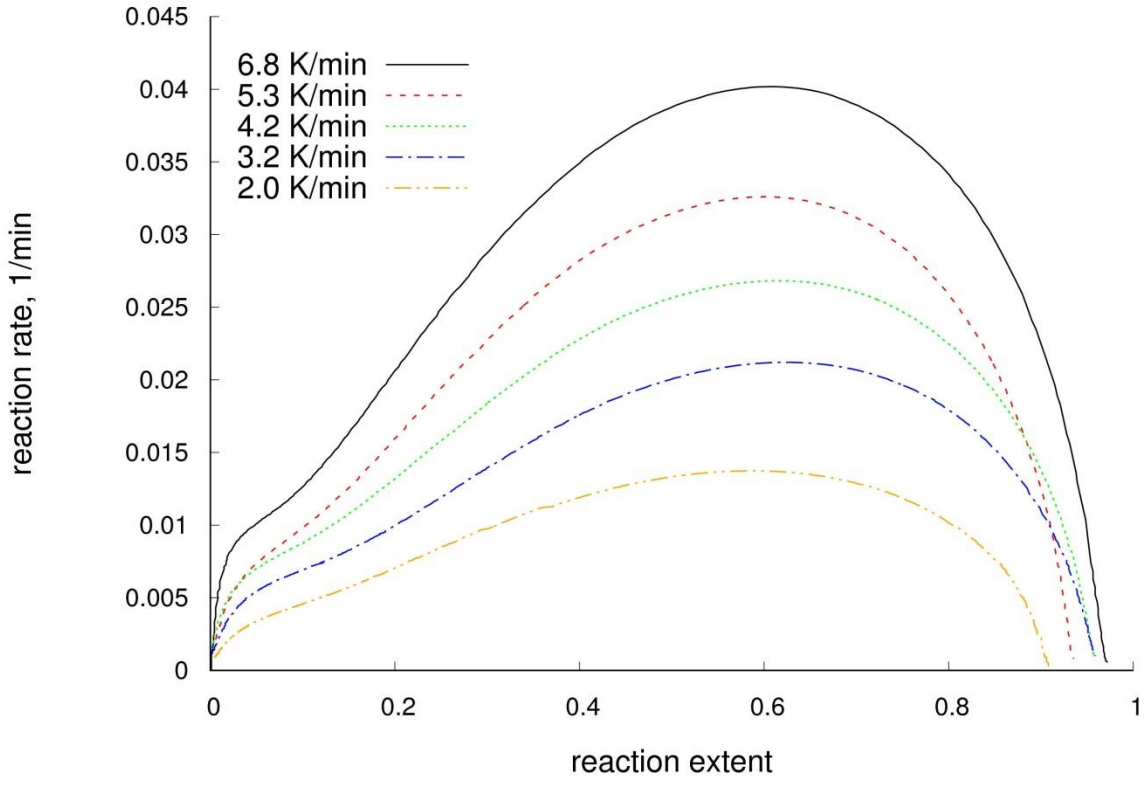

FIGURE S5. Average activation energy – average correlation coefficient plot for different models of powder reduction; vertical lines mark an expected activation energy range 65-95 kJ/mol; only models with av. correlation higher than 0.93 (17 from the group of 20) are shown

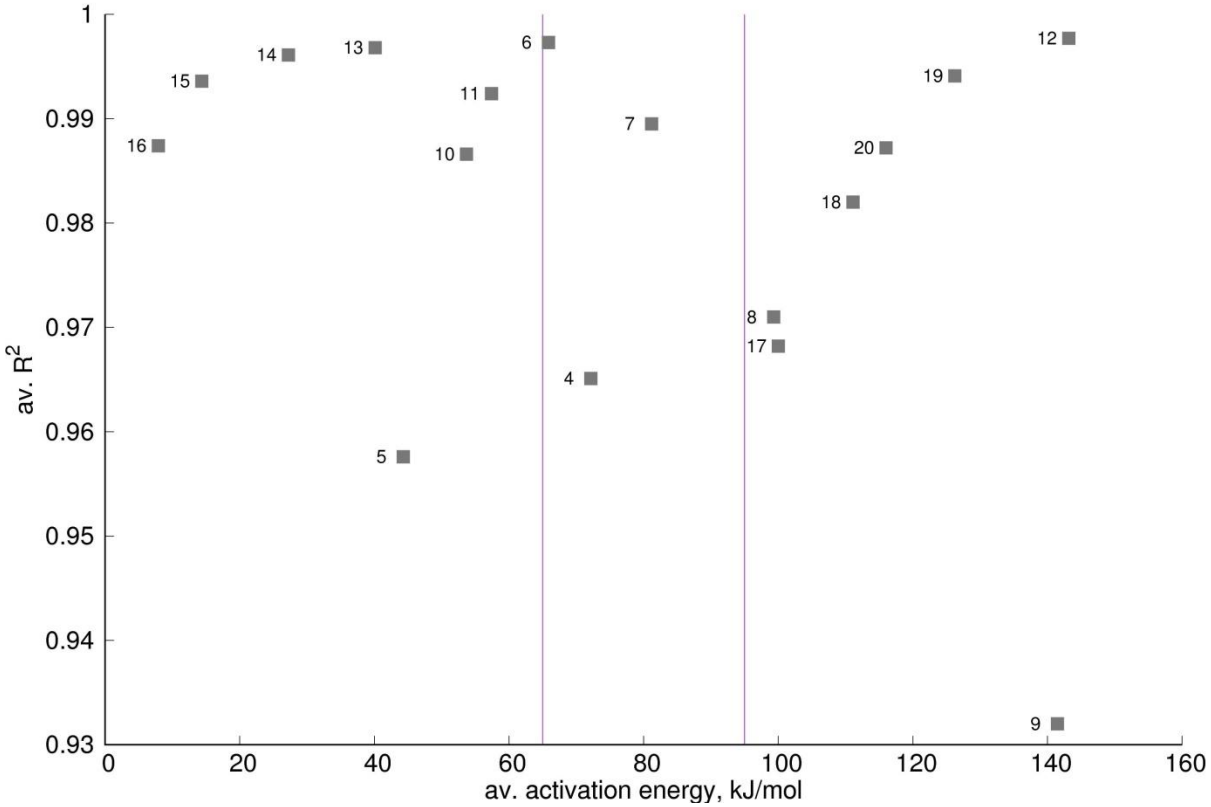

FIGURE S6. Average activation energy – average correlation coefficient plot for different models of pellet reduction; vertical lines mark an expected activation energy range 65-105 kJ/mol; only models with av. correlation higher than 0.93 (17 from the group of 20) are shown

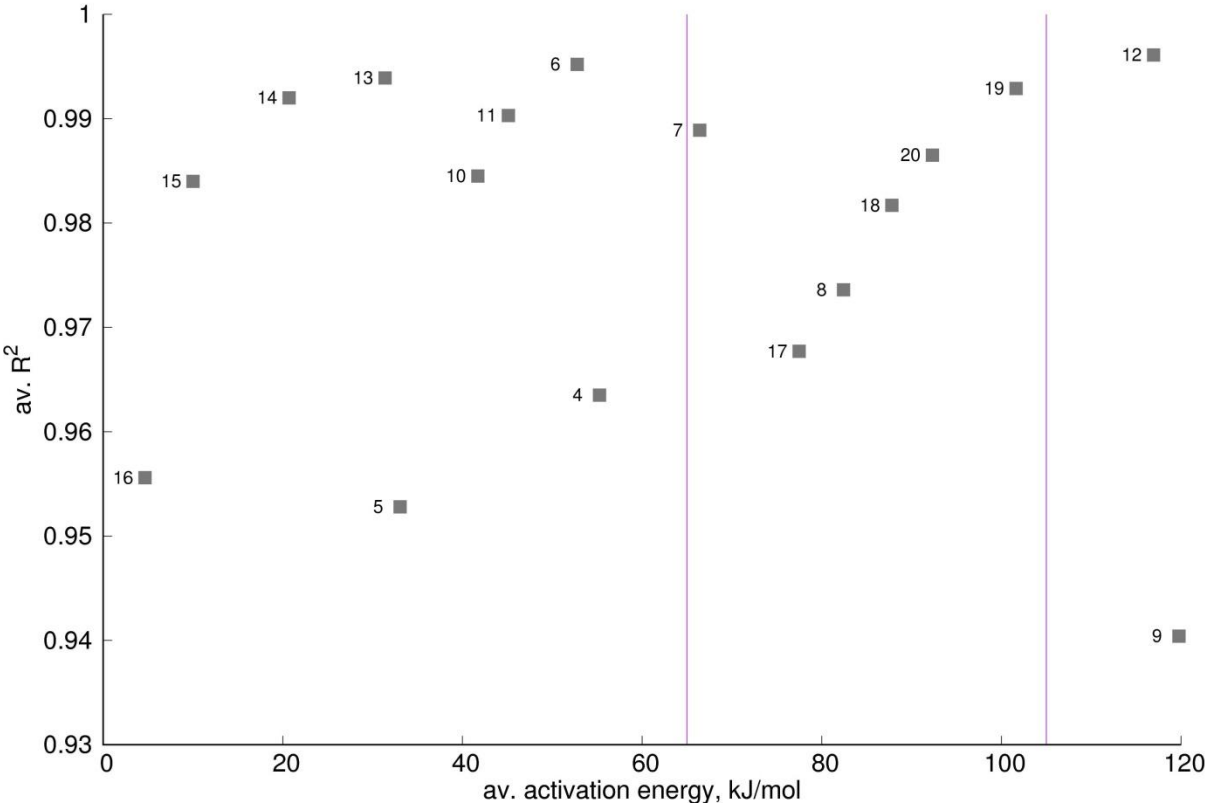

FIGURE S7. Dependence of the reaction extent on the reaction extent during a reduction of a milled nanometric powder in isothermal experiments; result for the initial micrometric powder are added for comparison.